

Advanced static and dynamic analysis method for helical springs of non-linear geometries

Zewen Gu^a, Xiaonan Hou^{a, *}, Jianqiao Ye^a

^a Department of Engineering, Lancaster University, Lancaster LA1 4YW, UK

Abstract

Current design and analysis methods of helical springs are significantly confined to a simple and linear domain. The traditional spring formula is only effective for analyzing helical springs with linear geometric properties like constant coil diameter, unchanged spring pitch and no coil contact. An advanced analytical spring model is proposed in this study to address the non-linear effects of variable coil diameter, spring pitch and coil contact that exist in helical springs of arbitrary shapes. It aims to expand the available spring design and analysis domain to a wider non-linear space. In addition, it is coupled with the modal spring model to explain and predict the dynamic vibrational response of non-linear helical springs. It is found that the proposed model has an excellent accuracy in estimating mechanical properties of non-linear springs in both static and dynamic conditions by comparing with experimental and FE results. This model may lead to an innovative method for developing innovative tools of spring design and performance analysis that could be beneficial to a wide range of engineering applications.

Keywords: Valve spring vibration, Non-linear helical geometry, Variable spring stiffness, Coil clash, Analytical model

1 Introduction

Helical springs are conventionally playing essential roles in many engineering applications, for instance, in valve train mechanisms [1] and vehicle suspension systems [2]. More recently, helical springs are also found able to make significant changes in the fields of sports science by increasing the top speed of human running [3, 4] and of biological science by investigating the evolutionary history of mantis shrimp using spring mechanics [5]. All these applications require fundamental geometrical descriptions of the helical springs. An accurate geometric representation always leads to a better design of helical spring, which can improve the performance of both the spring and the overall system, while an inaccurate representation may cause premature failure of the spring and the system. Therefore, the importance of representing the geometry of a helical spring should be properly addressed in both research and engineering applications. In fact, the development of analytical models for depicting spring geometries can be dated back to very early times.

Hooke's law is the first theory to describe the property of a normal helical spring, which defines the spring stiffness as the ratio of force and displacement. A fundamental and comprehensive study on helical springs was conducted by Wahl [6]. General formulas for calculating stiffness and natural frequency of a commonly used helical spring were proposed in his study. Researchers found these traditional formulas effective in static stress analysis of automobile springs [7], process control of coiling helical springs [8] and optimal design of helical springs made of either a metal material [9] or a composite material [10, 11]. Besides, these formulas

also contributed to the development of dynamical spring models, for instance, the multi-mass models and the distributed parameters models. In a typical multi-mass spring model, a helical spring is divided into several concentrated masses linked by linear connecting springs. For achieving accurate results, the stiffness of these connecting springs must be properly defined. Usually, the traditional spring formulas provide a fast and straightforward way to estimate the stiffness by averaging the overall stiffness of the helical spring [12-17]. A helical spring developed in the distributed parameters model is treated as parameters that are distributed across the entire spring body [18, 19]. The distributed parameter model assumes that the geometry of a helical spring consists of continuous and consistent elements. The geometric properties of the helical spring are then coupled with the dynamic equations to draw meaningful dynamic solutions. For example, in articles [20-22] where the method of superposition of vibration modes were applied, the traditional spring formulas were utilized efficiently to quickly obtain the value of the stiffness and natural frequencies of a helical spring. These results may draw a conclusion that the traditional spring formulas performed well in certain static and dynamic spring analysis. However, it was noted that the above helical springs were all linear, which means that these springs have linear geometric properties, such as a constant coil diameter, an infinite free length, and a constant pitch angle. However, these assumptions are extremely unrealistic in describing the geometries of helical springs that are used in most of the practical applications. In the vehicle suspension system, the suspension springs are usually grounded for the purpose of mounting [23, 24]. In addition, valve springs are intentionally designed to have varied spring pitch for the purpose of reduction of spring surge [25]. Moreover, unique spring designs, like beehive spring, conical spring and barrel spring, are all against the assumption of a constant coil diameter [26]. Applying the traditional spring formulas on these helical springs of non-linear geometric properties can bring unrealistic results.

In order to improve the design of helical springs further, spring models including these nonlinearities should be developed. One of the nonlinearities that exists in most of the common spring designs is the varying coil diameter. The helical springs with variable coil diameter are usually called non-cylindrical springs. Methods for representing these non-cylindrical springs were proposed in [26-29], where the methods were based on Love's spatial helix curve theory [30]. The investigated geometric shapes in these studies were restricted to three types: barrel, conical and hyperboloid. In other words, although contain variable coil diameters these springs are still relatively simple and of linear geometry. Additionally, spring designers have looked for better mechanical performance by altering the cross section of spring wire to make it non-circular. It was found that different shapes of cross section did not introduce extra computational efforts because that non-circular cross sections still have a constant moment of inertia as long as they are uniform across the whole spring wire [31, 32]. As a result, the constant moment of inertia did not increase the complexity of the governing equations for calculating spring properties. Another possible nonlinearity existing in helical springs is the effects of the grounded ends or the non-uniform ends. These non-uniform ends are usually designed for the purpose of mounting, where half or more than half of the end coils are cut off. It is unrealistic to treat them as normal active coils as they are always closed when they are in service conditions. These parts can be considered as fixed rotational springs that are connected to the main spring body [33, 34]. Another convenient way is to discount the end coils when counting the number of active coils [25]. No significant differences between the two methods have been reported.

Traditional spring formulas showed poor predictions to the non-linear features of helical springs. Existing extension theories based on the traditional spring formulas are effective but can only work well with spring of simple shapes, such as conical (Figure 1a), barrel (Figure

1b) and hyperboloid (Figure 1c) which have relatively simple variation of coil diameters (Figure 1d).

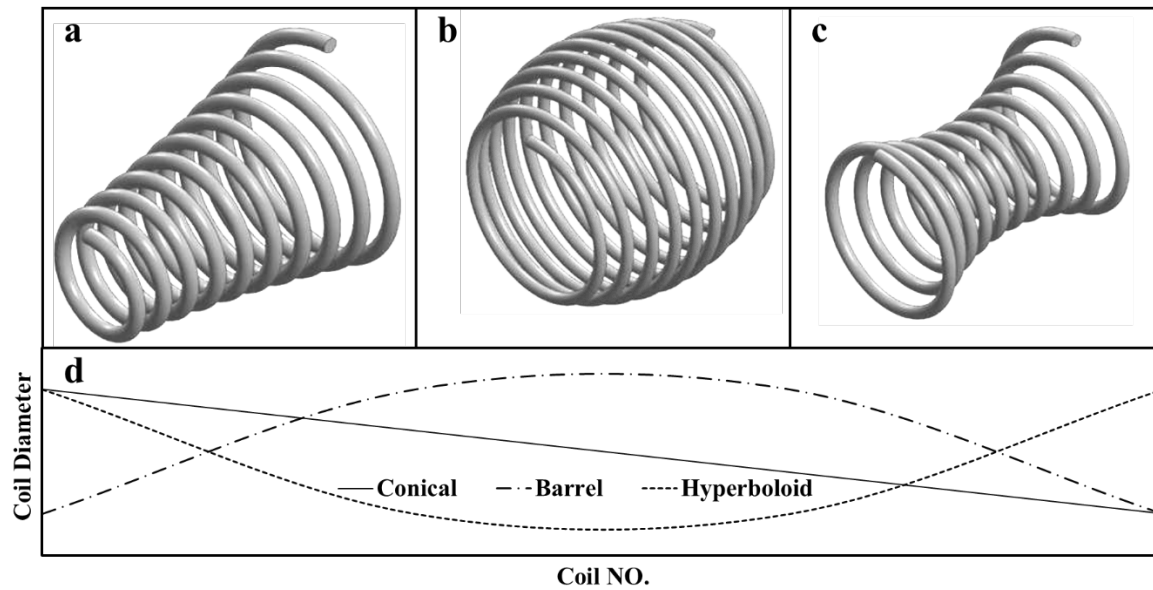


Figure 1: Normal non-cylindrical shapes of helical springs (a). Conical, (b). Barrel, (c).Hyperboloid and (d).The relationships between their coil diameters and coil number.

More importantly, to the authors' best knowledge, no existing study has investigated the effects of coil contacts on the calculations of spring stiffness and natural frequency. As a result, there is a lack of methods and knowledge on the analysis and design of non-linear springs. Besides, the lack also becomes a barrier for the analysis of the system response in high-speed dynamic systems that use non-linear helical springs. In this paper, the spring formulas for calculating spring stiffness and natural frequency are derived by considering the helical spring as an assembly of many curved beam elements. The theories of the formulas are extended to include the non-linear geometric properties of helical springs. The aim is to include the effects of variable coil diameter, variable pitch and end coils in the proposed model, while at the same time to ensure the efficiency and accuracy of the model. The results obtained from spring compression tests and FE (finite element) modelling are used to validate the static analytical results. Additionally, the present spring model is coupled with a distributed parameter model of spring to explain and analyze the dynamic response of the spring at high operation speeds, which is validated by the results of a high-speed engine test and of the dynamic FE spring model.

2 Analytical Model

2.1 Traditional spring formulas based on curved beam theory

In an early study of Wahl [6], spring formulas were proposed based on assuming the spring as a uniform curved beam. Figure 2 shows a sketch of a normal cylindrical spring that is compressed by a force F and produces displacement x . It assumes that a small beam element has a length dl , and the compression causes a torsional moment T on the curve element. The torsion of the element results in a longitudinal displacement dx , and the overall spring displacement x is the sum of all the dx of every beam element. According to these assumptions, the mass of each beam element dm is written as:

$$dm = \frac{\pi d^2 \rho dl}{4g} \quad (1)$$

where d is the wire diameter of the spring, ρ is the density of the spring material and g is the acceleration of gravity. The overall mass of the spring m is then calculated by:

$$m = \int_0^m dm = \int_0^{N \cdot \pi D} \frac{\pi d^2 \rho dl}{4g} = \frac{\pi^2 d^2 \rho ND}{4g} \quad (2)$$

where N is the number of spring coils and D is the constant coil diameter. According to Wahl's theory and the torsional theory of beam, the stiffness of the spring k is given by:

$$k = \frac{Gd^4}{8D^3N} \quad (3)$$

where G is the shear modulus of the spring material. To calculate the fundamental natural frequency, a helical spring is always assumed to be fixed at both ends of the spring. The fundamental natural frequency f of the helical spring is expressed as the stiffness k and the spring mass m .

$$f = \frac{1}{2} \sqrt{\frac{k}{m}} = \frac{d}{\pi D^3 N} \sqrt{\frac{Gg}{2\rho}} \quad (4)$$

Eq.(3) and Eq.(4) are the fundamental and widely used equations for researchers and spring designers. They are convenient and efficient for calculating stiffness and natural frequency of a conventional helical spring with a uniform coil diameter D , a fixed number of active coils N and a constant spring pitch. Clearly, the application of the formulas are rather restrictive, as helical springs with linear geometries are only a subgroup of a wide range of spring types, most of which are with non-linear geometries. Moreover, even a spring with designed linear properties may exhibit non-linear behaviours as a result of errors introduced from the manufacturing process. Thus, the development of an analytical model capable of accurately estimating non-linear spring properties is essential and practically meaningful.

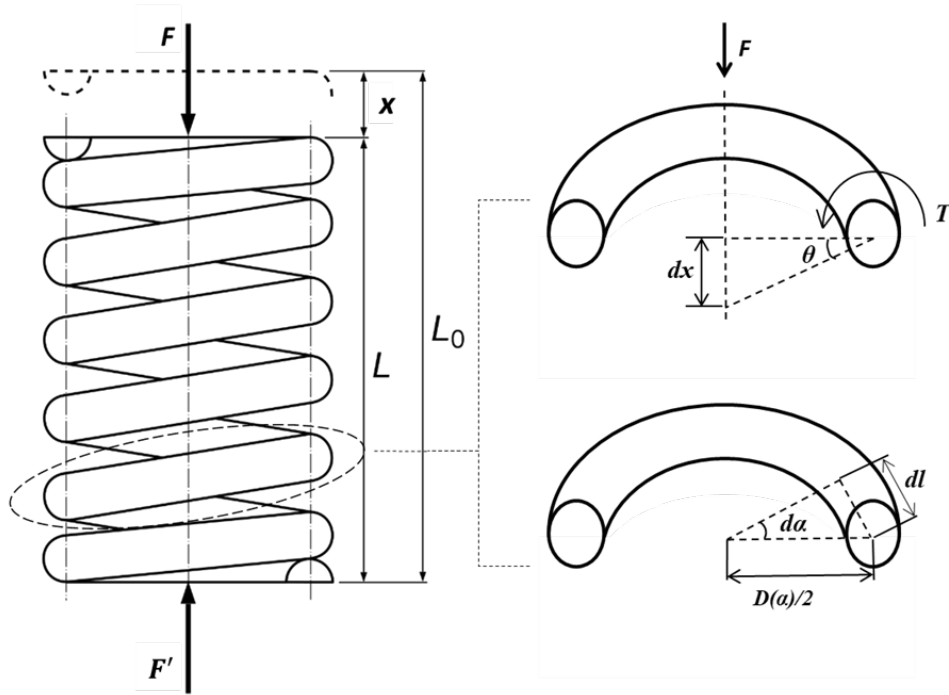


Figure 2: Sketch of a conventional helical spring and the load conditions of spring coils.

2.2 Spring formula considering variable coil diameter

One of the non-linear properties that should be included is variable coil diameter. A constant coil diameter generates cylindrical helical springs, while a variable coil diameter may produce helical springs of conical, barrel or hyperboloid shape, and any other desirable shapes. Based on Wahl's basic assumption, a helical spring is treated as a curved beam which is formed by infinitesimal beam elements. Each beam element has a uniform length dl and orientates along the helix angle $d\alpha$ as shown in Figure 2. When the helical spring is subjected to an axial compression F , each beam element is assumed to have an axial displacement dX , which can be calculated by:

$$dX = \frac{D(\alpha)}{2} \cdot \theta \quad (5)$$

where α denotes the helix angle, θ is the torsional angle of the spring element caused by the compressive force F , and $D(\alpha)$ is a function of α which is no longer a constant and denotes the variable coil diameter. The length of the spring element can be defined by:

$$dl = \frac{D(\alpha)}{2} \cdot d\alpha \quad (6)$$

According to the formula of beam in torsion, for the beam of length dl :

$$\frac{T}{J} = \frac{G \cdot \theta}{dl} \quad (7)$$

where the torsional moment T is:

$$T = F \cdot \frac{D(\alpha)}{2} \quad (8)$$

and the polar moment of a circular cross section is J :

$$J = \frac{\pi d^4}{32} \quad (9)$$

where d denotes the diameter of the wire cross section. Substituting Eq.(6), Eq.(7), Eq.(9) and Eq.(10) into Eq.(8) yields the expression for the displacement of each spring element as:

$$dX = \frac{4FD(\alpha)^3 d\alpha}{G\pi d^4} \quad (10)$$

From this equation, it can be seen that the displacement of each spring element is not uniform but changes with the coil diameter. In order to calculate the overall displacement at the moving end of the spring X , integration of Eq.(10) is taken over $[0, X]$, i.e.,

$$X = \int_0^x dX = \frac{4F}{G\pi d^4} \int_0^{\alpha_0} D(\alpha)^3 d\alpha \quad (11)$$

Then, according to Hooke's law, the stiffness of the spring can be written as:

$$k = \frac{F}{X} = \frac{G\pi d^4}{4} \cdot \frac{1}{\int_0^{\alpha_0} D(\alpha)^3 d\alpha} \quad (12)$$

In the above equations, α_0 represent the total helix angle of a specific helical spring. It differs depending on the design of a spring, but it has a fixed relationship with the number of active coils N_a , i.e., $\alpha_0 = 2\pi N_a$. Hence, Eq.(12) can be also written as a function of the number of active coils N_a by:

$$k = \frac{F}{X} = \frac{G \cdot \pi \cdot d^4}{4} \cdot \frac{1}{\int_0^{2\pi N_a} D(\alpha)^3 d\alpha} \quad (13)$$

The new stiffness formula in this section includes the effect of variable coil diameter by introducing a coil diameter function $D(\alpha)$. Similar to Wahl's theory, the formula assumes that the torsional effect plays the most essential role, and the bending and shear effects of the spring are neglected. In addition, the formula assumes a constant helix angle (a constant number of active coils N_a). Hence, the new formula Eq.(13) is suitable for springs having symmetric spring pitch whose coils usually do not contact with each other. A new stiffness formula for considering both variable coil diameter and variable spring pitch is presented in the next section.

2.3 Spring formula considering both variable coil diameter and variable spring pitch

Traditional helical springs are usually designed to have a constant spring pitch in many engineering applications. However, as the development of new spring design, asymmetric pitch is increasingly adopted in the design of helical springs. These springs are found having many advantages in various applications. For instance, in a suspension system, a narrow pitch makes the spring stiffer after a certain compression and in a valve train mechanism the closing coils can increase the natural frequency of the valve spring and therefore reduce the maximum dynamic forces. The stiffness formula in the previous section is then modified here to include the effect of narrow pitch. Firstly, Eq.(11) is rewritten in a generalized form to show the time-dependent effect:

$$X(t) = S_f \cdot F(t) \cdot \int_0^{\alpha_0} D(\alpha)^3 d\alpha \quad (14)$$

where the S_f is a constant and is as below:

$$S_f = \frac{4}{G\pi d^4} \quad (15)$$

As the effect of the narrow pitch changes with loading time, the force F also changes with time. It is because that spring stiffness changes at the loading steps when coils collide. Hence, the spring displacement $X(t)$ is considered as a function of time step t . In Eq.(14), the lower limit of the integral is zero, representing the first spring element of the fixed spring end and the upper limit $\alpha\theta$ denotes the last spring element of the moving end of the spring. However, when coil contacts are considered, the lower and the upper limits of the integral should be, respectively, the first untouched spring element of the fixed and the last untouched spring element of the moving end. Hence, Eq.(14) is rewritten as:

$$X(t) = S_f \cdot F(t) \cdot \int_{\alpha_i(t)}^{\alpha_e(t)} D(\alpha)^3 d\alpha \quad (16)$$

where $\alpha_e(t)$ and $\alpha_i(t)$ represent the helix angles of the first and the last untouched spring elements, respectively. To determine α_e and α_i , the function of spring pitch $P_t(\alpha)$ with respect to the helix angle α is introduced. This function represents the value of the spring pitch of the infinitesimal spring element at helix angle α . The theory is that the closed coils of both the lower and the upper end of the spring are treated as isolated helical springs. Then the displacements of these isolated helical spring are calculated by:

$$X_i(t) = S_f \cdot F(t) \cdot \int_0^{\alpha_i(t)} D(\alpha)^3 d\alpha \quad (17)$$

$$X_e(t) = S_f \cdot F(t) \cdot \int_{\alpha_e(t)}^{\alpha_0} D(\alpha)^3 d\alpha \quad (18)$$

In Eq.(17) and Eq.(18), $X_i(t)$ and $X_e(t)$ denote the displacements of the isolated springs at the fixed end and the moving end, respectively.

Figure 3 shows a helical spring that is subjected to a time dependent loading $F(t)$. The loading $F(t)$ results in a displacement at the upper end of the helical spring $X(t)$. Under this loading, several coils begin to contact with other coils. Then, these contacted coils at the upper and the lower ends are considered as isolated springs 1 and 2, respectively, in Figure 3, where P_{t_i} and P_{t_e} represent the sum of the pitches of the contacted coils at the same vertical position of the last untouched spring elements. Therefore, they are calculated, respectively, by:

$$P_{t_i}(\alpha_i(t)) = \sum_{n=0}^{\lfloor \frac{\alpha_i(t)}{2\pi} \rfloor} P_t(\alpha_i(t) - 2\pi n) \quad (19)$$

$$P_{t_e}(\alpha_e(t)) = \sum_{n=0}^{\lfloor \frac{\alpha_0 - \alpha_i(t)}{2\pi} \rfloor} P_t(\alpha_e(t) - 2\pi n) \quad (20)$$

where $P_t(\alpha)$ is the function of the spring pitch with respect to helix angle α . $\lfloor \cdot \rfloor$ is a rounding down function to the nearest integer.

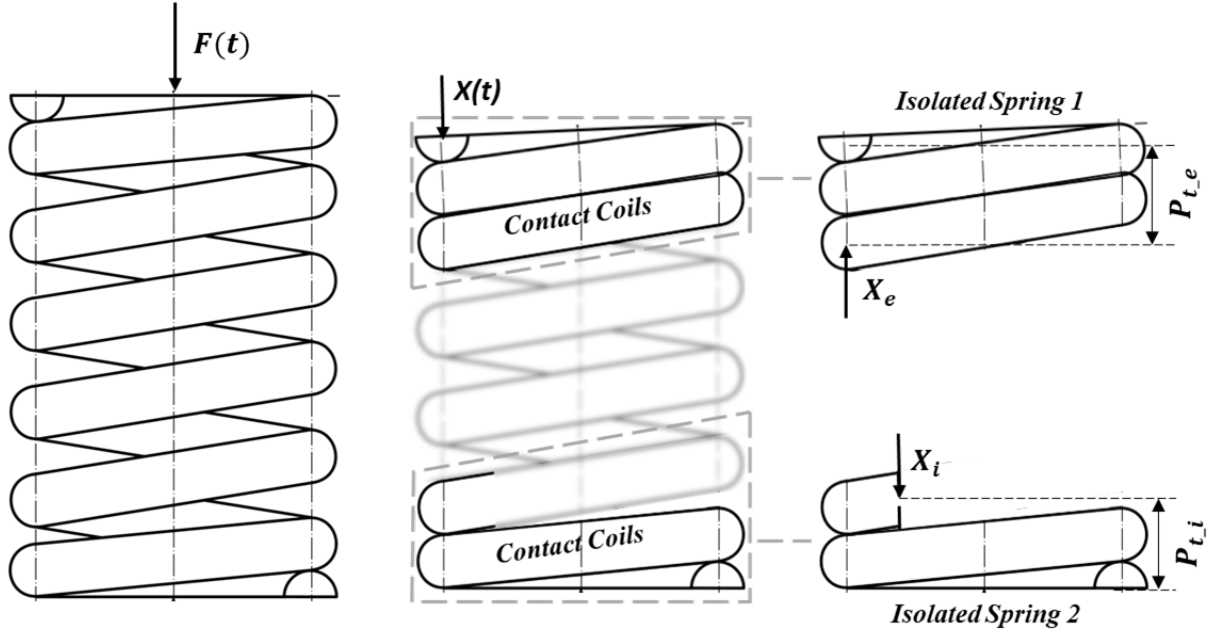


Figure 3: Sketch of the closed spring coils under compressions which are treated as isolated springs.

The displacements X_i and X_e of the isolated springs 1 and 2 should be equal to the total pitch values P_{t_i} and P_{t_e} , respectively. In other word, coils are closed when they satisfy that:

$$X_i(t) = P_{t_i}(\alpha_i(t)) \quad (21)$$

and

$$X_e(t) = P_{t_e}(\alpha_e(t)) \quad (22)$$

Then, α_i and α_e can be obtained by solving the above two equations. By substituting $\alpha_i(t)$ and $\alpha_e(t)$ into Eq.(16), the function of displacement $X(t)$ considering closed coils can be obtained. Eventually, the stiffness function is obtained by applying Hooke's Law as:

$$k(t) = \frac{F(t)}{X(t)} = \frac{1}{S_f \cdot \int_{\alpha_i(t)}^{\alpha_e(t)} D(\alpha)^3 d\alpha} \quad (23)$$

It can be seen that the stiffness $k(t)$ is now a function of time t instead of a constant after considering the effects of closing coils. It is because that at each loading time step the number of closed coils or the number of active coils may be different so that the stiffness changes accordingly.

3 High-Speed Dynamic Spring Model

In the real world, helical springs serve for a category of working conditions. Most of them are subjected to a low-speed or high-speed dynamic motion. This covers a large range of spring types, one of which is the most typical valve spring. The valve spring normally works in a valve train mechanism, which is an essential part of a car engine. It works in both low- and high-speed conditions, where the engine speed can reach as high as 10000 RPM. It has been widely known that a static spring model is not sufficient to represent these dynamic effects, and therefore dynamic spring models are required by the industry. In an early study of Wahl [6], an analytical dynamic spring model was proposed based on the distributed parameter method. In the model, the dynamic response of a helical spring is assumed as a superposition of dynamic motions of the spring at every vibrational mode. The motions of the spring is

described by a partial differential equation Eq.(24) which is in the same form to the one-dimensional wave equation.

$$\frac{\partial^2 y(x, t)}{\partial t^2} = c^2 \frac{\partial^2 y(x, t)}{\partial x^2} \quad (24)$$

where $c = l\sqrt{k/m}$ denotes the speed of wave propagation across the spring; l , k and m are the length, stiffness and active mass of a spring respectively; $y(x, t)$ is the displacement of a spring element at position x and time t . Following his study, Philips et al.[20] presented a detail strategy for solving this dynamic spring model. Firstly, the lower end of the spring is assumed fixed when the upper end is free. Then, the motion of a spring is assumed to have two components, i.e., a static response and a dynamic response. With these assumptions, Eq.(24) becomes:

$$\frac{\partial^2 s_d(x, t)}{\partial t^2} = c^2 \frac{\partial^2 s_d(x, t)}{\partial x^2} - \frac{l_0 - x}{l_0} \cdot \frac{d^2 z(t)}{dt^2} \quad (25)$$

where l_0 is the free length of the spring and $z(t)$ is the displacement of the moving end caused by the loading. $s_d(x, t)$ denotes the dynamic contribution which is a function of both x and t . On the other hand, the dynamic term $s_d(x, t)$ can be treated as harmonic in time [35], and its free solution is a separable form:

$$s_d(x, t) = f(x)e^{i\omega t} \quad (26)$$

When $f(0) = f(l_0) = 0$ is the boundary condition, the ordinary differential equation can be solved as:

$$f(x) = \sin\left(\frac{n\pi x}{l_0}\right) \text{ when } n = 1, 2, 3, \dots \quad (27)$$

The relationship $\omega/c = n\pi/l_0$ can be found as $f(l_0) = \sin(\omega \cdot l_0/c) = 0$. An efficient way to solve the dynamic equation is to assume the solution as a superposition of the independent vibration modes [20-22]. Then, the dynamic term can be written as:

$$s_d(x, t) = \sum_n S_n(t) \sin\left(\frac{n\pi x}{l_0}\right) \quad (28)$$

where $S_n(t)$ is the dynamic amplitude of the spring at the n -th frequency. In addition, the coefficient of this term can be also written as a Fourier expansion in terms of the above modes:

$$\frac{l_0 - x}{l_0} = \sum_n \frac{2}{n\pi} \sin\left(\frac{n\pi x}{l_0}\right), \text{ where } 0 < x < l_0 \quad (29)$$

By using this method, the dynamic equation is transformed from a partial differential equation to a set of ordinary differential equations. However, these equations have not considered the internal damping of the spring which plays an essential role in accurately estimating the dynamic vibration of spring [25, 36]. Therefore, a viscous damping term is added into Eq.(25) and it becomes:

$$\frac{d^2 S_n(t)}{dt^2} + 2\xi\omega_n \frac{dS_n(t)}{dt} + \omega_n^2 S_n(t) = -\frac{2}{n\pi} \cdot \frac{d^2 z(t)}{dt^2} \quad (30)$$

where ξ is the viscous damping ratio of a spring. For solving $S_n(t)$ from the equation, a Fourier solution method is used in this paper. The application of this method can be also found in the studies of [21, 22]. Firstly, time t is replaced by the cam speed ω_{cs} and the cam angle φ , so that $dt = d\varphi/\omega_{cs}$. Hence, Eq.(30) can be rewritten as:

$$\frac{d^2 S_n(\varphi)}{d\varphi^2} + 2\xi \frac{\omega_n}{\omega_{cs}} \cdot \frac{dS_n(\varphi)}{d\varphi} + \frac{\omega_n^2}{\omega_{cs}^2} S_n(\varphi) = -\frac{2}{n\pi} \cdot \frac{d^2 z(\varphi)}{d\varphi^2} \quad (31)$$

Then, $S_n(\varphi)$ and the applied load $d^2 z(\varphi)/d\varphi^2$ can be written in the form of Fourier series:

$$S_n(\varphi) = \sum_{i=0}^{\infty} (p_i \cos(i\varphi) + q_i \sin(i\varphi)) \quad (32)$$

$$\frac{d^2 z(\varphi)}{d\varphi^2} = \sum_{i=0}^{\infty} (a_i \cos(i\varphi) + b_i \sin(i\varphi)) \quad (33)$$

where a_i , b_i , p_i and q_i are the coefficients of Fourier series. By substituting Eq.(32) and Eq.(33) into Eq.(31), p_i and q_i can be computed from :

$$p_i = \frac{-2a_i/n\pi - 2q_i\xi\omega_n i/\omega_{cs}}{\omega_n^2/\omega_{cs}^2 - i^2} \quad (34)$$

$$q_i = \frac{-2b_i/n\pi - 2p_i\xi\omega_n i/\omega_{cs}}{\omega_n^2/\omega_{cs}^2 - i^2} \quad (35)$$

The dynamic equation can be obtained now by solving the p_i and q_i . Eventually, the total dynamic spring force can be considered as a sum of the dynamic force F_d and the static force F_s . The dynamic force is caused by the internal vibrations of the spring, and it has the relationship with $S_n(\varphi)$ as:

$$F_d = \pi k \sum_n n S_n(\varphi) \quad (36)$$

The static force F_s is generated by the static compression of spring, which consists of a pre-load x_p and an external load $z(\varphi)$. So, the static force can be obtained by:

$$F_s = k (x_p + z(\varphi)) \quad (37)$$

It is noteworthy that the k in Eq.(36) and Eq.(37) is the spring stiffness which is currently a constant. However, as what was explained in the previous section, the spring stiffness could be variable during the process of compression and vibration when the spring has non-linear geometric properties. Therefore, a more general solution for the spring force can be obtained by replacing the constant stiffness k by a variable stiffness $k(\varphi)$. As a result, the total dynamic spring force F can be calculated by:

$$F = F_s + F_d = k(\varphi) (x_p + z(\varphi)) + \pi k(\varphi) \sum_n n S_n(\varphi) \quad (38)$$

4 Numerical Example

4.1 Geometry and material

To validate the efficiency of the developed non-linear spring formulas, a beehive spring is used as an example in this section. The beehive spring (Figure 4a) is manufactured by Force Technology Ltd. and serves in the high-speed engine of sports cars. Figure 4b, c, d and e depict the wire diameters, coil diameters, spring heights and spring pitches based on the design specifications and 3D scanning measurement, respectively. Apart from the wire diameter, small discrepancies in the spring height and the coil diameter are observed between the design

specification and the actual geometry from 3D scanning. It is because that, usually, a helical spring is designed to have a linear geometry, as described by the traditional spring formulas. However, errors can be introduced in the process of manufacturing, which may result in geometrical nonlinearities. Hence, the geometry model used in this paper is developed according to the scanning data, which could assure a more realistic prediction of the springs.

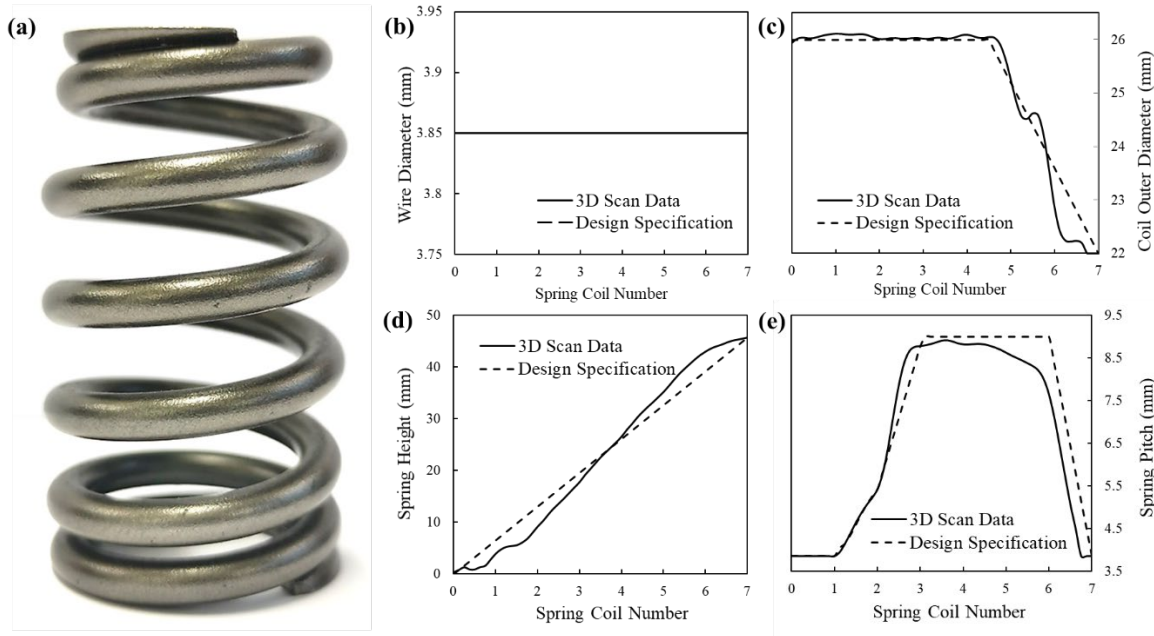


Figure 4: (a). Real beehive spring product and its geometry based on 3D scan technique and design specifications of (b). wire diameter, (c). coil diameter, (d). spring height and (e).spring pitch. Adapted from [37].

The material used to fabricate the beehive spring is super clean spring steel with the type code of Oteva 90. It is a widely used steel for manufacturing springs with high fatigue properties and excellent relaxation properties. Table 1 shows the mechanical properties of the material.

Table 1: Mechanical properties of super clean spring steel Oteva 90.

Physical properties

Wire (mm)	Tensile strength (N/mm ²)	Modulus of elasticity (GPa)	Modulus of shear (GPa)	Poisson's ratio
3.85	2080-2180	206	79.5	0.29

4.2 Static compression experiment and dynamic engine head test

In practice, the beehive spring is produced for using in valve trains and acts as valve spring. It performs to ensure the opening and closing process of intake and exhaust valves accurately. In this case, the beehive spring is always pre-compressed by 7mm in the valve train. Figure 5(a) shows the 7mm compression test that is conducted by Force Technology Ltd. Then the reaction force of the spring is recorded. The contact status of the spring coils at 1mm, 3mm and 7mm compression are displayed in Figure 5(b), Figure 5(c) and Figure 5(d) respectively. It demonstrates that the spring pitch between the first and the second coils is progressively compressed and eventually the second coil contacts the first coil fully at 7mm compression.

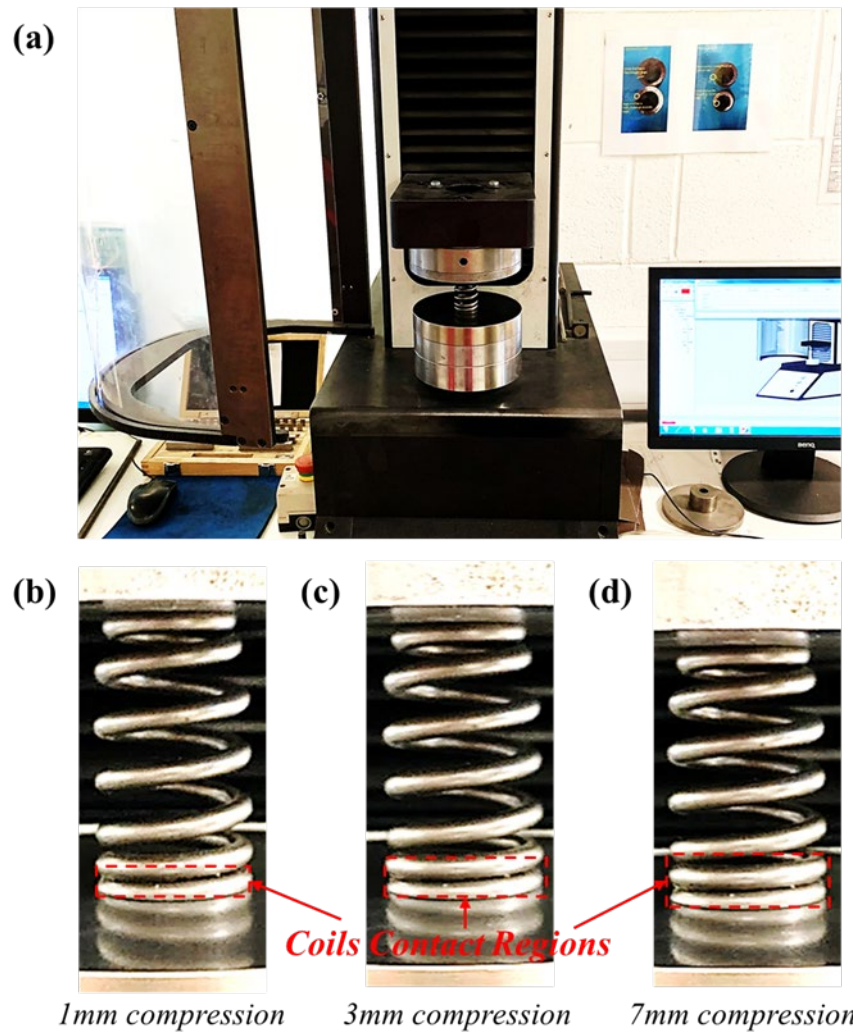


Figure 5: (a). The 7mm compression test conducted on the beehive valve spring sample, and the contact status of spring coils at (b).1mm, (c).3mm and (d).7mm compression obtained from the testing result. Adapted from [37].

Besides working in static conditions, the beehive spring mainly works in high-speed dynamic conditions. As a valve spring, it is always seated in the valve train of the engine head as shown in Figure 6. The engine head is the essential part of the V8 car engine of sports cars. In the engine, the beehive spring will bear high-speed dynamic loadings, which can be in the range of 2000-8000 rpm. As for testing the dynamic spring force at various engine speeds, an engine test of the McLaren V8 engine is conducted as shown in Figure 7. The whole engine is motivated, and the engine speed is controlled by the external electrical motor. For monitoring the reaction force of the beehive valve inside the engine, a sensor is placed at the bottom surface of the spring. Then, the motor rotates at various speeds that makes the engine working as it does in a real sports car. The output dynamic spring forces is compared with finite element results and analytical results in following sections.

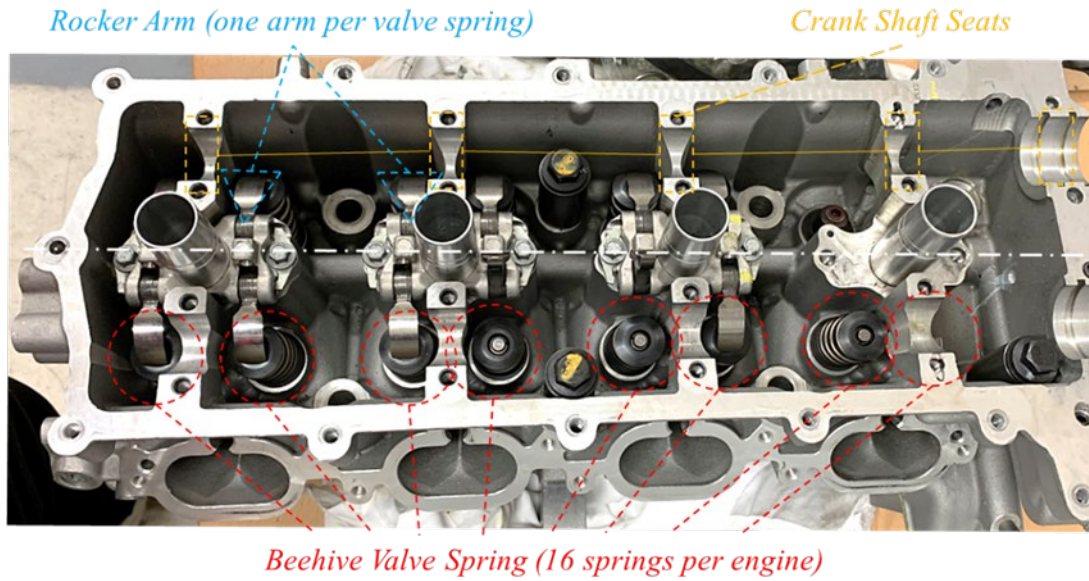


Figure 6: Engine head of the sports car.

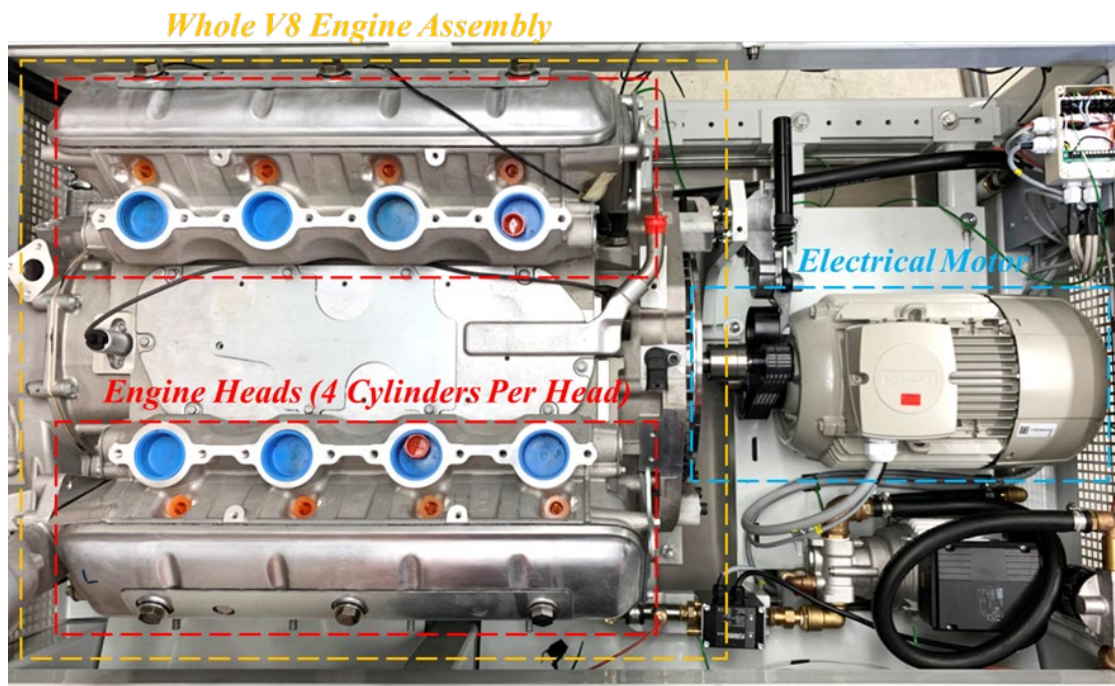


Figure 7: Speed controlled engine test rig for the V8 engine of the sports car.

4.3 Finite Element Spring Model

A numerical spring model based on FE method is used in this paper in comparison with the developed analytical model and experiment. Firstly, the geometry of the spring is generated based on the 3D scan data. The 3D model is then imported into and meshed by the commercial software Ansys. The detailed meshing strategy and experimental validations of the FE spring model can be found from the authors' previous study [38]. The FE model is shown in Figure 8(a) where the lower end face B of the spring is fixed and the upper end face A is subjected to a 7mm longitudinal compression as shown in Figure 8(b). In addition, self-contact is also defined across all the spring coils, which enables the consideration of coil clash. These conditions simulate the practical working conditions of the beehive spring in a valve train. The

first and last end coils are meshed by tetrahedron elements in order to better fit the irregular shapes. On the contrary, the coils in the middle range are meshed using hexahedron elements for reducing the mesh density while ensuring the accuracy. In total there are 70475 elements with 160500 nodes in the meshed spring model. Static FE simulations are then conducted, and they are used to validate the proposed analytical model together with the experimental results in the following sections. The dynamic FE simulation applied the same geometric model of the spring. The loading of the dynamic simulation is corresponding to the displacement of the cam profile as shown in Figure 12a. The detail setting of the dynamic FE model can also be found in the previous study [38].

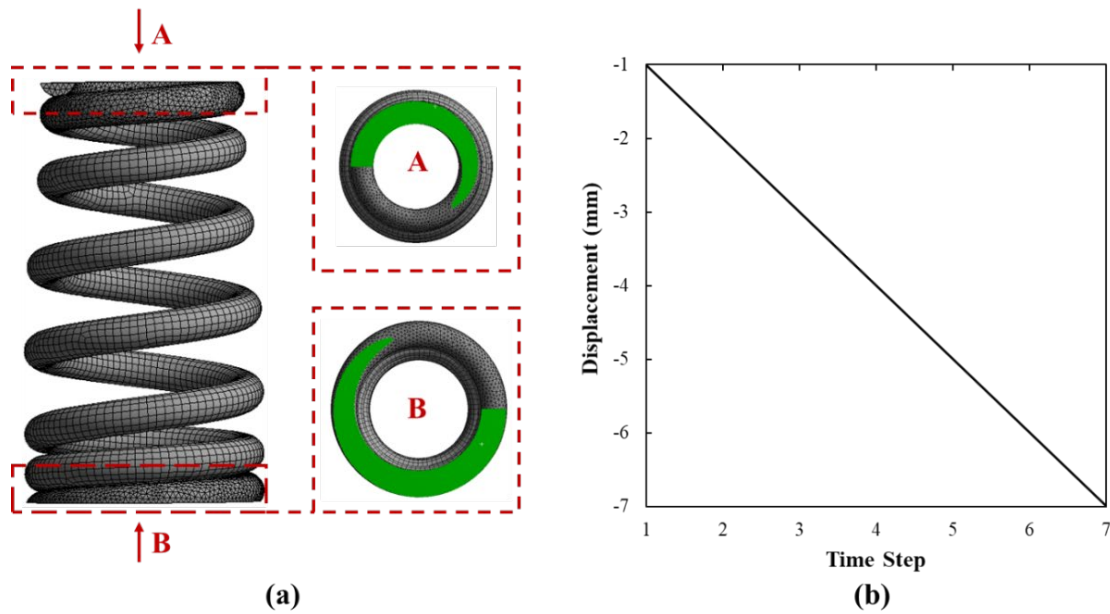


Figure 8: (a). FE spring model meshed by commercial software Ansys and (b). 7mm compression loading. Adapted from [37].

4.4 Static response with consideration of non-linear spring geometries

The proposed spring formula in this article is applied to analyze the mechanical properties of the beehive spring. As stated in the previous sections, the beehive spring has geometrical nonlinearities (varying coil diameter and changing spring pitch). In order to consider these factors, firstly, an expression that can fit the 3D scan data of the coil diameter and spring pitch should be found. In this study, the least squares polynomial fit method achieved by the Python package ‘NumPy’ is employed to regress the fitting functions. This method aims to find the minimum variance between the values from the regression function and the values of the scan data. A fit degree is usually introduced to regulate the length and the dimension of the regression polynomial expression. In other words, the value of the fit degree represents the maximum order and the number of terms of the regression polynomial expression. A low fit degree may fail to fit the data points while a high fit degree always results in higher computational efforts.

Figure 9(a) and Figure 9(b) shows the regression functions of the varying coil diameter and the changing spring pitch by using the least square polynomial method. When the orders of fit degree are below 10, the fitting curves of both the coil diameter and the spring pitch show obvious mismatch with the 3D scan data. When the order of fit degree is raised to 15, it appears that the regression polynomials functions can fit the scanned coil diameter and spring pitch curves very well. Therefore, the order of fit degree for fitting both the coil diameter and the spring pitch curves are chosen to be 15 in this paper. Next, the regression function of spring

pitch P_t is used to construct the function of pitch summation P_{t_i} and P_{t_e} in Eq.(19) and Eq.(20). The fitting quality of the constructed P_{t_i} and P_{t_e} is shown in Figure 9(c) by comparing with the summation of the 3D scan spring pitch data. It can be seen that an order of fit degree 15 is sufficiently high for fitting the scan data. In the beehive spring of this study, only the lower portion of the spring has damping coils (have narrow pitches). Therefore, it is assumed that during the 7mm compression only the coils at the lower portion will be closed progressively. Thus, the solutions of the Eq.(21) should be determined at different loadings steps. Figure 9(d) depicts the relationships between the curves of X_i and $P_{t_i}(\alpha_i)$ under various loading steps. The X_i curve has no intersections with the $P_{t_i}(\alpha_i)$ curve at a spring force of 100 N, which makes Eq.(21) have no solution. It means that the spring coils have not contacted with each other at this loading step. When the spring force increases to 220 N, the X_i curve has one intersection with the $P_{t_i}(\alpha_i)$ curve at around 1rad helix angle. The contacting helix angle α_i can be therefore solve from Eq.(21), which is used to determine the current number of active coils N_a . When the spring force reaches 320 N, the X_i curve has more than one intersection with the $P_{t_i}(\alpha_i)$ curve. The intersections at the largest helix angle (around 5.5 rad) is the last contact spring element, and all the spring elements at helix angles smaller than it are assumed to be in full contact. The proposed analytical spring model was implemented and solved in the open source integrated development environment (IDE) Spyder by coding in Python.

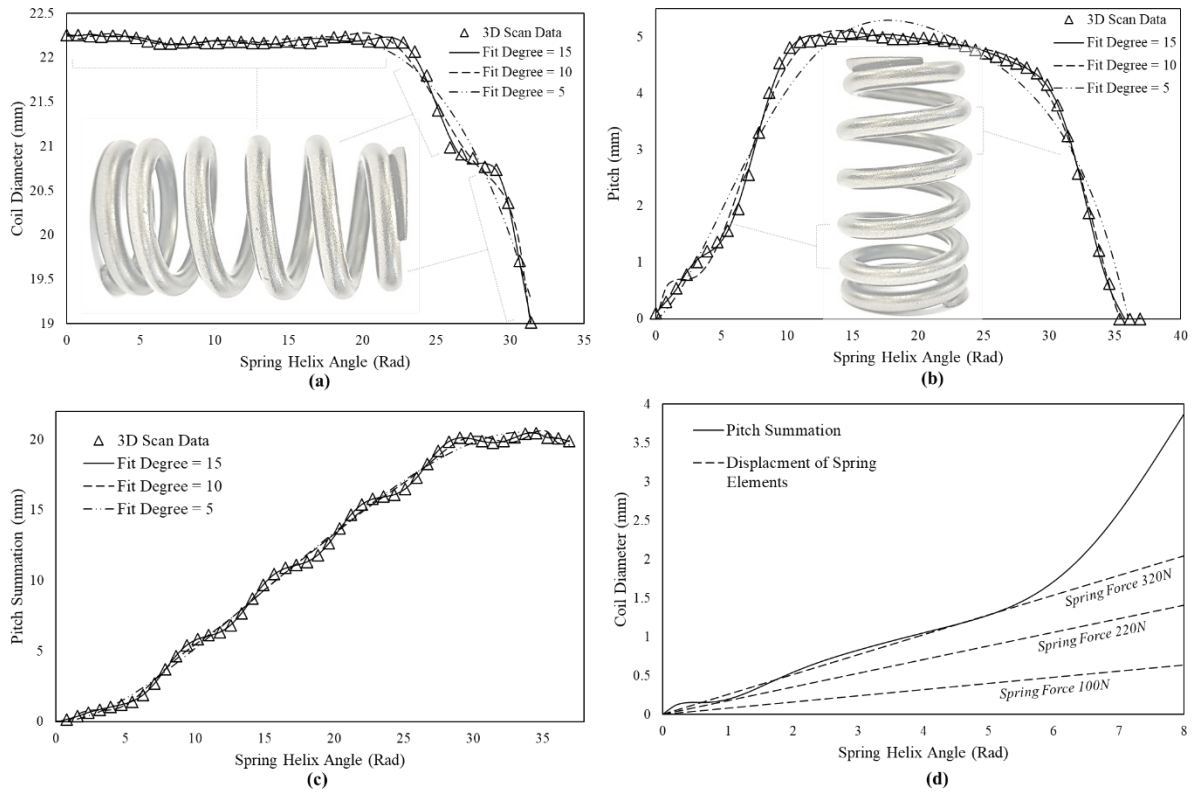


Figure 9: Polynomials functions with 5, 10 and 15 fit degree for fitting the 3D scan data of (a). coil diameter, (b). spring pitch and (c). summation of pitch. And (d). position of contact coils at different loading step.

Then, the function $D(\alpha)$ for fitting the coil diameter curve and the helix angle of the last untouched spring element α_i can be substituted into the proposed spring formula, and the spring stiffness can be calculated by considering the effects of variable coil diameter and changing spring pitch. The compression force of the beehive spring estimated by the traditional analytical formula, by the proposed analytical formulas considering only variable spring pitch, only variable coil diameter and considering both variable pitch and variable coil diameter are

presented in Figure 10. In addition, the experimental results and the FE results are also plotted to validate the analytical results. A significant discrepancy can be observed between the results based on the traditional spring formula and others. At 7 mm compression, the force can only reach approximately 210 N according to the traditional spring formula, while it is around 312 N from the experimental and FE simulation results. It is mainly because that the reduced size of the spring coils at the upper portion and the narrowed pitch at the lower portion of the beehive make the spring stiffer, which cannot be considered by the traditional formula. As a result, the traditional formula that assumes a constant coil diameter and pitch underestimate the spring force significantly when comparing with the experimental results. For the analytical model that considers variable pitch only, the calculated spring force is around 270 N at 7 mm compression which is slightly lower than the experimental and the FE results. However, the result is closer to the experimental results than the ones obtained from traditional formula. It is because that the spring stiffness becomes higher during compression with the consideration of the closed spring coils. The relative higher stiffness results in a higher spring force. Similarly, the proposed spring formula considering only the variable coil diameter estimates the spring force around 280 N at 7 mm compression, which is slightly higher than the results obtained by the formula considering variable pitch only. It is noted that this curve has a good agreement with the experimental and the FE results before 5 mm compression. However, the deflection is much bigger, when the compression is between 5 mm and 7 mm. as shown in Figure 11 that is a zoomed view of the compression between 5 mm and 7 mm. This phenomenon is due to the contacts between the coils with narrow pitch, i.e., when the compression exceeds 5 mm, these coils become closed coils. Consequently, the actual number of active coils is reduced, which increases the overall stiffness of the spring.

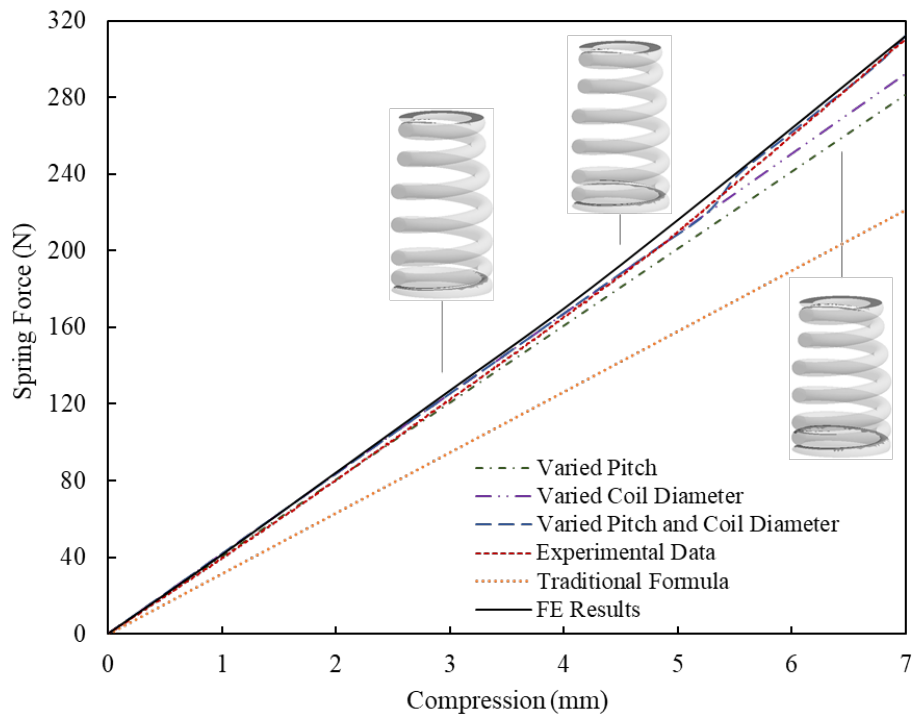


Figure 10: Spring force curves under a 7 mm compression based on experimental data, FE analysis, traditional spring formula and proposed analytical models considering varied pitch and/or varied coil diameter.

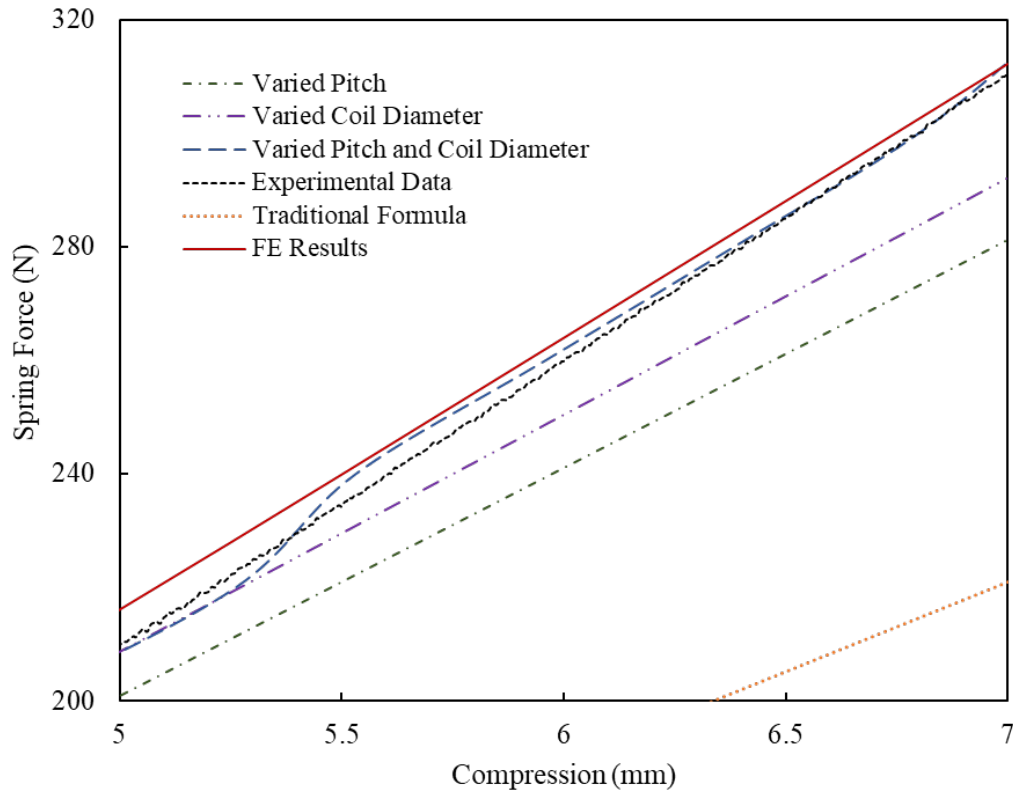


Figure 11: Spring force curves under a 7 mm compression based on experimental data, FE analysis, traditional spring formula and proposed analytical models considering varied pitch and/or varied coil diameter. (Zoom in area between 5 mm and 7 mm compression)

The proposed spring formula, which considers the effects of both variable coil diameter and coil contact, shows its strong ability to estimate the force of non-linear spring during compression. At 7 mm compression, the calculated spring force is approximate 314 N, which is very close to the results of the experiment (312 N) and the FE analysis (312 N). In addition, the curve of the force fits very well with the FE and the experimental curves during the overall compression process (0 mm to 7 mm). It demonstrates that the proposed spring formula has the ability to accurately estimate the mechanical properties of a helical spring. Especially, when the helical spring has high non-linear geometries, for instance, variable coil diameter and narrow pitches, the proposed formula still can give an accurate prediction when the traditional spring formula fails to do so.

4.5 High-speed dynamic response with consideration of variable spring stiffness

In addition to the non-linear performances of helical springs under static loading conditions, the dynamic properties of the beehive spring are also of great importance in practice. However, the existing analytical dynamic models are mainly based on the springs with linear geometries, which are not capable to predict the dynamic force of a non-linear spring. This section shows the dynamic results of the beehive spring by coupling the developed spring formulas with the distribute parameter spring model.

As per the development of analytical model for predicting the dynamic performances of springs with non-linear geometries in Section 3, the dynamic effects of a helical spring are composed of a static term and a dynamic term as shown in Eq.44. The developed analytical model is coded using the scientific packages ‘Symfit’ and ‘Numpy’ in the open source software Python. In the analysis, the beehive spring is pre-compressed by 7 mm to simulate the assembly in a

real valve train system, which should provide enough force to close the valve. So, a 7mm preloading is firstly added into the model. Then, the dynamic input is derived from the profile of the cam over the spring. The cam rotates when the engine works, and it executes displacement on the top of the spring. The dynamic loading applied in the analytical model is shown in Figure 12(a) which shows the displacement of one cycle of cam rotation. As a result of the displacement, the varying stiffness of the beehive spring $k(\varphi)$ during the cam cycle is shown in Figure 12(b) which is calculated using Eq.(23). These results are imported to the developed dynamic analytical model in Eq.(38) to calculate the dynamic spring force.

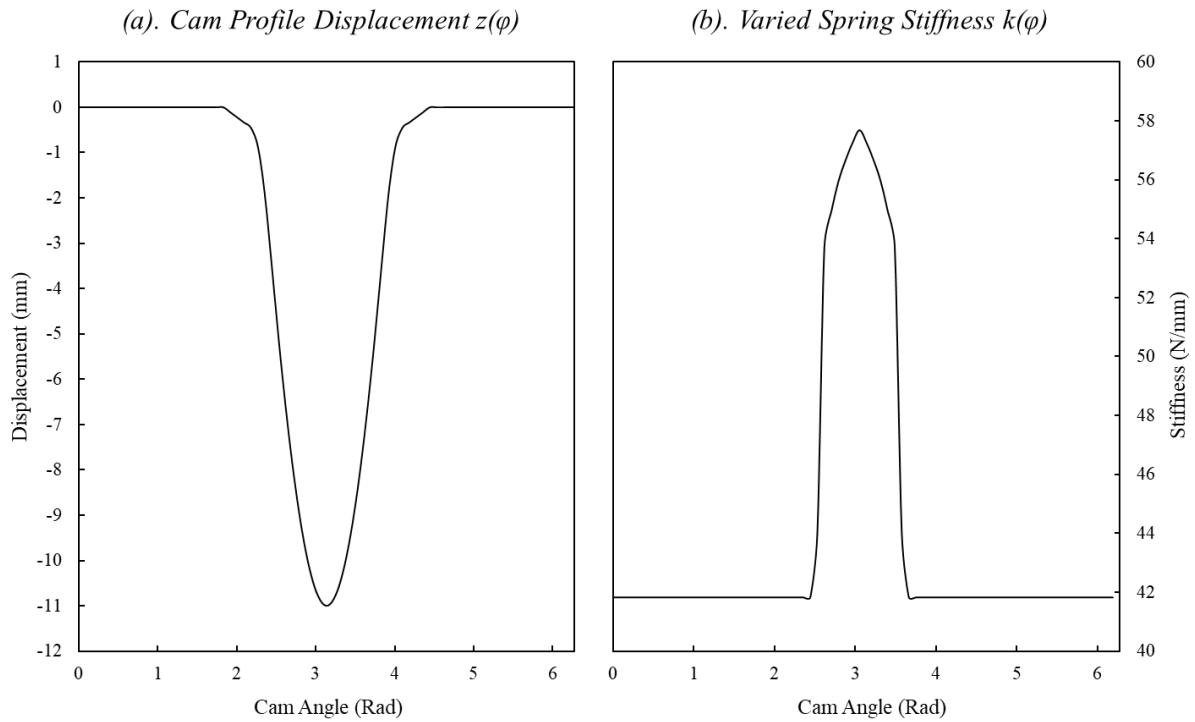


Figure 12: (a). The cam profile of the valve train mechanism. (b). The varied spring stiffness of the beehive spring respect the angle of the cam.

As demonstrated in Section 3, the first step for calculating the dynamic spring force is to find the dynamic amplitude, $Sn(\varphi)$, of each vibration mode n . The first simulated engine speed is 4000-rpm which equals to 2000-rpm cam speed. Firstly, the external loading $z(\varphi)$ is input to Eq.(33) to calculate the Fourier coefficients a_i and b_i . The damping ratio ζ is 0.016 and the first order natural frequency ω_1 is 631 Hz which are the same as the ones in the finite element model. The dynamic amplitude $Sn(\varphi)$ can be obtained by substituting the inputs a_i , b_i , ζ and ω_1 into Eq.(34) and Eq.(35) to solve q_i and p_i . Figure 13(a) - (e) display the modal vibrations of the first five vibration modes $n \cdot Sn(\varphi)$ respectively.

The cam profile displacement $z(\varphi)$ in Figure 12(a) demonstrates that there is no external loading applied to the spring at 0-2 rad and 4.5-6.28 rad. However, the spring still has modal vibrations at each mode especially at the first mode $n=1$ as shown in Figure 13. It is because that the spring experience free vibration as for dissipating the residual dynamic energy at 4000-rpm engine speed. At approx. 2.5 rad and 4.2 rad, the cam starts to compress the spring, the vibration status of the spring experience a sudden change and short pulses are generated at each mode as shown in Figure 13. In addition, it is observed that the vibrations between 2.5 rad and 4.2 rad have larger amplitudes than free vibrations as the spring under an external loading from the cam. According to Eq.(38), the effects of the dynamic responses of all the vibration mode will be added onto the static response of the spring (Figure 13(f)). In addition, it is noted that the

vibration contributes less to the overall dynamic response, when the mode of the vibration is higher. Therefore, only the vibrations of the first five mode are considered in the analytical model in this study.

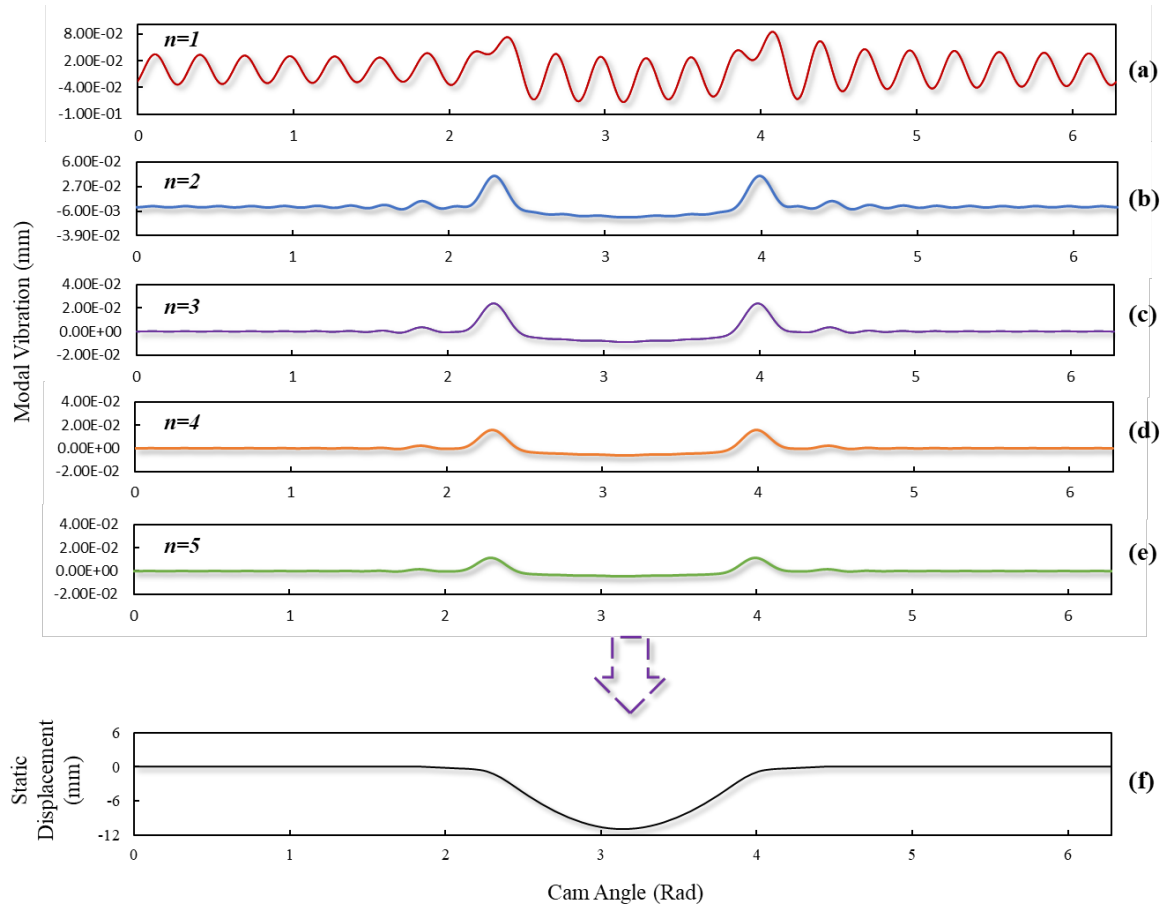


Figure 13: The modal vibrations of the beehive spring of modal modes (a). $n = 1$, (b). $n = 2$, (c). $n = 3$, (d). $n = 4$ and (e). $n = 5$ at 4000-rpm engine speed respectively. And the static displacement of the upper end of the spring caused by cam rotation.

The overall dynamic force of one cam cycle at 4000-rpm engine speed is shown in Figure 14, which can be calculated by using Eq.(38). The results of the engine head test and the dynamic FE simulation are also plotted to validate the developed analytical model. Throughout the entire cam cycle, both the analytical and the FE results have a good agreement with the test data. The spring force starts with approx. 312 N, which is the result of the 7 mm pre-load. The tested spring force has a slight fluctuation between 0 rad and 2 rad, which indicates that the energy from the last cam cycle has not been completely dissipated and the spring is under free vibration. In addition, the spring force shows similar vibrations between 4 rad and 6.28 rad. This is caused by the cease of the external loading at 4 rad and the spring experience free vibration again. The analytical model can simulate the free vibrations of the spring well at the two stages. From 2 rad to 3.14 rad, the tested force increases gradually, and it drops after the peak force around 851 N at 3.14 rad to about 310 N again at 4 rad. This process is caused by the cam profile which reaches its largest displacement (11 mm) at 3.14 rad. During this stage, the analytical model can also fit the test result well as shown in Figure 14. The comparisons between the forces from the analytical model, the engine head test and the FE model illustrate that the spring already has detectable vibrations, when working under cycling loadings at around 4000-rpm engine speed. More importantly, the analytical model proves its ability for accurately and quickly

predicting the magnitude of dynamic force and the existence of spring vibrations, which performs as well as the dynamic FE model does.

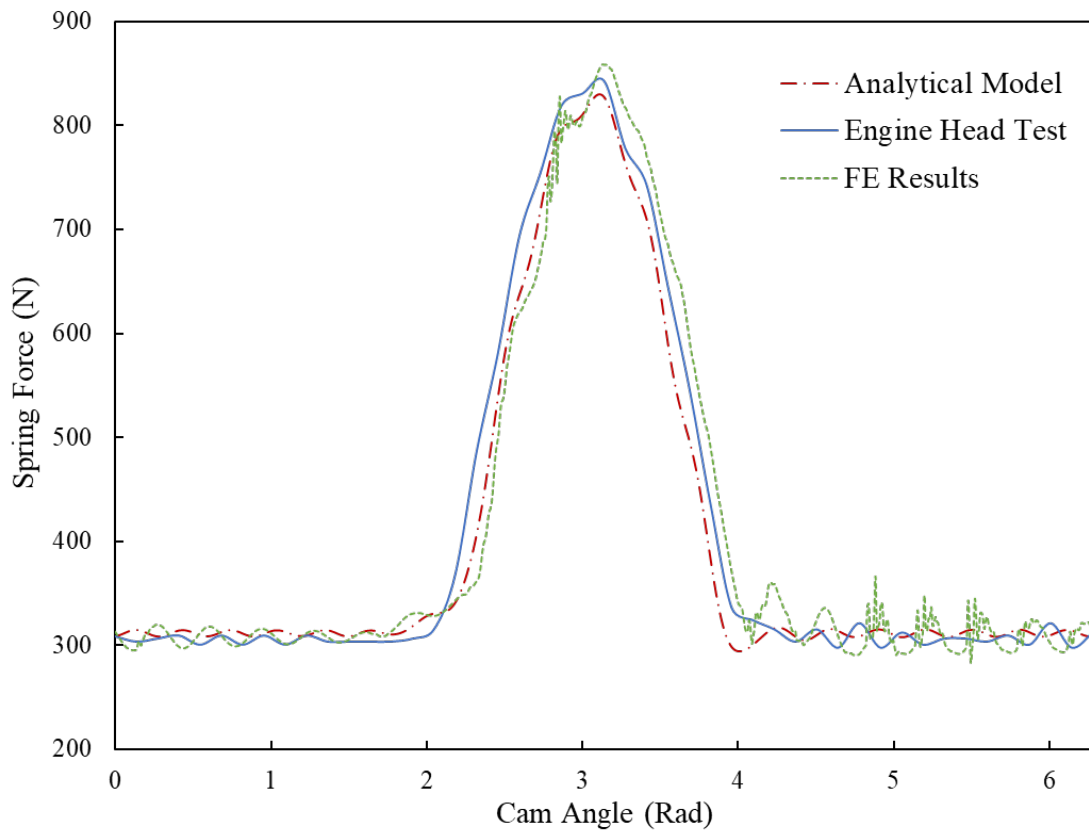


Figure 14: The comparison between the dynamic forces of the beehive spring within one cam cycle at 4000-rpm engine speed based on the analytical model, engine head test and dynamic FE model.

The analytical model is also used to simulate the dynamic spring force of the spring at higher engine speed 5600-rpm. It is easy to calculate that 5600-rpm is 1400-rpm higher than 4000-rpm in terms of engine speed, and 700-rpm higher in terms of cam speed. Hence, the parameters of the analytical model are unchanged despite increasing the cam speed to 2700-rpm. The modal vibrations of the first five modes at 5600-rpm are shown in Figure 15(a) - Figure 15(e) respectively. At the first mode $n=1$, the largest amplitude of the vibration can reach around 0.5mm, which is significantly larger than 0.08mm at 4000-rpm. It is reasonable as the higher engine speed actually results in higher vibrational energy. In addition, it is observed that the period of one vibration cycle at 5600-rpm is shorter than that at 4000-rpm. It is because the higher engine speed decreases the time for every cam cycle. It is also noteworthy that 5600-rpm is, when compared with 4000-rpm, closer to the second order natural frequency which is around 1262 Hz. It explains the phenomenon that the second mode $n=2$ at 5600-rpm shows more obvious vibration (Figure 15b) than that at 4000-rpm does (Figure 13b). Besides, the fifth mode vibration contribute very little to the overall dynamic response at 5600-rpm, which is similar to the phenomenon at 4000-rpm engine speed. (Figure 15(e)). Eventually, the dynamic vibration of each mode can be accumulated and added on the static displacement (Figure 15f).

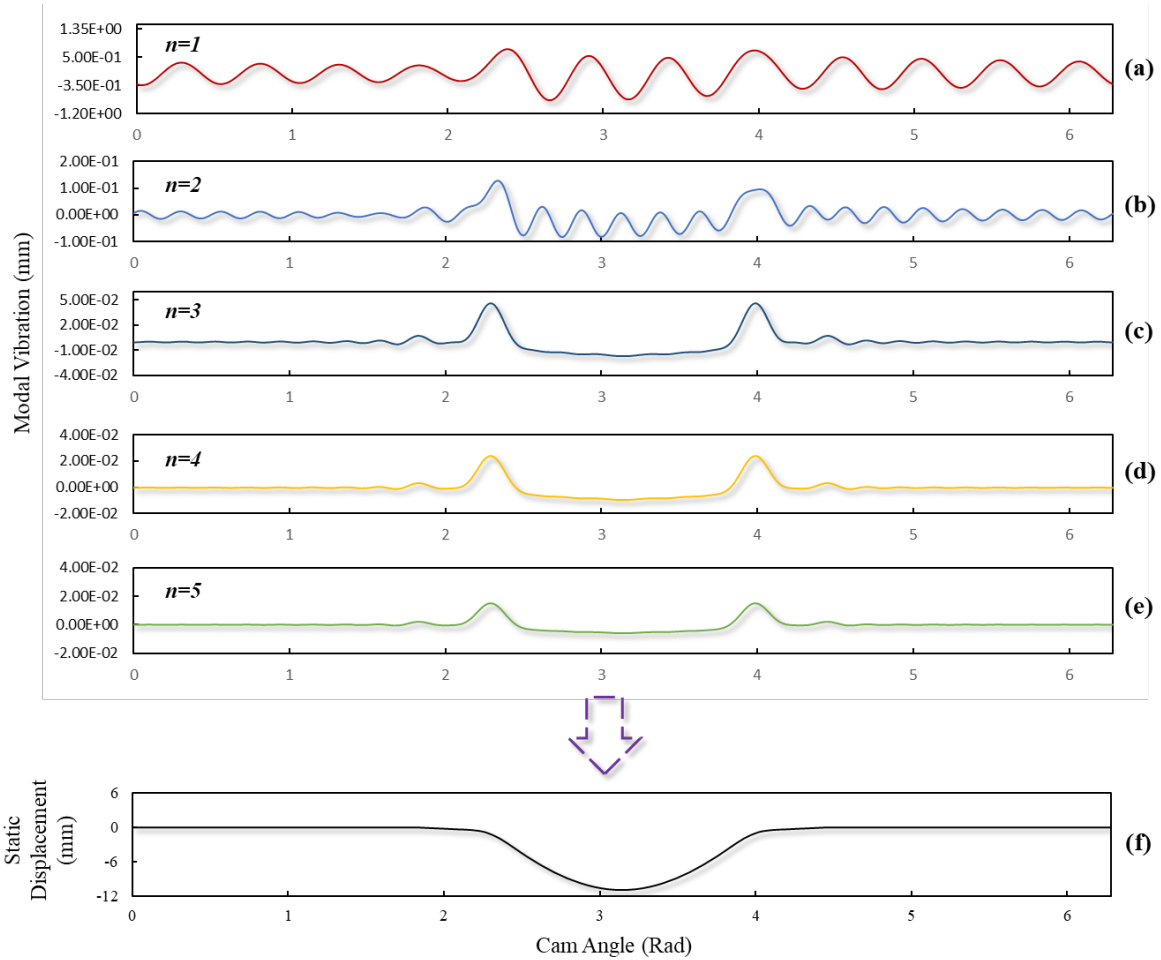


Figure 15: The modal vibrations of the beehive spring of modal modes (a). $n = 1$, (b). $n = 2$, (c). $n = 3$, (d). $n = 4$ and (e). $n = 5$ at 5600-rpm engine speed respectively. And the static displacement of the upper end of the spring caused by cam rotation.

The overall dynamic force of the beehive spring at 5600-rpm is plotted in Figure 16 together with the results of the engine head test and the dynamic FE model. When the engine speed reaches 5600-rpm, the internal vibration of the spring becomes more significant no matter at either the stage of free vibration (0 rad – 2 rad and 4 rad – 6.28 rad), or the stage of forced vibration (between 2 rad and 4 rad). To be specific, the largest vibration amplitude at free vibration stage can reach approx. 100 N (from 250 N to 350 N) compared to approx. 10 N at 4000-rpm engine speed. After 2 rad, when the spring is under external compression of the cam, the spring force starts to increase gradually. However, the force has a sudden drop at around 2.9 rad and then increases again until reaching the peak force 849 N from the test, 841 N from the analytical results and 890 N for the FE results at 3.14 rad. A similar phenomenon can be also observed at approx. 3.4 rad, when the spring force reverses to increase during the process of decreasing. In addition, it is noted that there is a rapid change of the spring force at around 4.2 rad. This phenomenon is caused by the impacts between the narrow coils at the fixed end. The reasons and details of the phenomenon have already been explained and discussed in another paper [38]. After the forced vibration, the spring comes into the second free vibration stage after 4.2 rad. It can be concluded that the analytical model has successfully predicted the dynamic force of the beehive spring, which is as accurate as the FE model, even when the engine speed is increased to a higher speed of 5600-rpm.

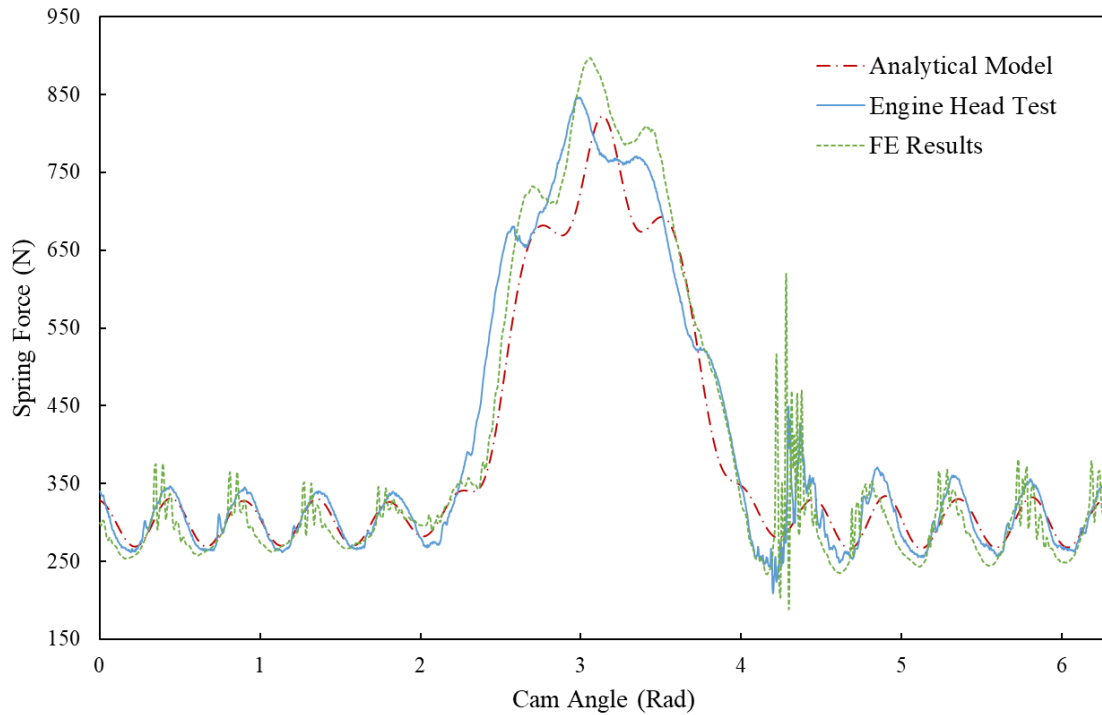


Figure 16: The comparison between the dynamic forces of the beehive spring within one cam cycle at 5600-rpm engine speed based on the analytical model, engine head test and dynamic FE model.

With consideration of variable spring stiffness caused by coils contacts, the developed analytical model can accurately predict the dynamic spring force of the beehive spring at different engine speeds, which is validated by both the test data and the FE results. It is also found that the dynamic response of the spring at 5600-rpm is more significant than the dynamic response generated at 4000-rpm. The analytical results demonstrate that the amplitude of the dynamic vibrations of each mode are increased when the engine speed increase due to increment of the accumulated dynamic vibration of all the vibration modes.

5 Conclusion

This paper presents an analytical spring model for predicting both static and dynamic mechanical properties of helical springs of non-linear geometries. Unlike the conventional cylindrical helical springs, these springs contain highly non-linear geometries: variable coil diameter and pitches. The proposed model shows the robust ability to deal with these nonlinearities while the traditional spring formulas fail to. Hence, it provides a solid fundamental for further analyzing static, dynamic or impact responses of non-linear springs, especially when coil clashes exist. The main findings can be concluded as follow:

1. It is found that a practical beehive spring usually has highly irregular geometries, such as variable coil diameters and pitches. 3D scanning data of the helical spring can better describe the non-linear geometry of a real beehive spring as it includes the tolerance from the manufacturing process. In this article, the non-linear geometry is represented by two polynomial functions of order 15. The good representation of helical geometries provides a solid foundation for accurately predicting mechanical properties of non-linear helical springs under both static and dynamic loadings
2. The developed analytical model is successfully validated by both the experimental data and the FE models. The mechanical performances of the spring are analyzed by comparing the

results of traditional spring model, the developed analytical model, the FE simulation and the experimental data. In static analysis, it is found that the traditional spring model is unable to analyze the helical springs with non-linear geometric properties (varied coil diameter, narrow pitch and coil contacts). It is due to its linear assumption that helical springs always have a constant coil diameter and number of active coils, so that the spring stiffness is linear during compression. On the contrary, the developed spring formulas can accurately estimate the mechanical properties of non-linear helical springs as accurate as the FE analysis does, which are all validated by the experimental result. **Therefore, the developed model can replace FE dynamic models in practice to save computational resources and is potentially helpful for developing a real-time controlling system in manufacturing for the industry.** More importantly, the developed analytical model significantly expands applicable parameters of spring geometries to a larger domain in spring design, in addition to its capability of analyzing the nonlinearity. It makes it possible to include variable pitch and diameters of individual coils in design as tuneable parameters, which cannot be considered in the current design practice.

3. In dynamic analysis, the developed spring model is coupled with the analytical modal spring model to simulate the dynamic response of the non-linear beehive spring. The results show that the developed dynamic spring model can well predict the dynamic force of the spring by considering the non-linear properties of the spring. At both 4000-rpm and 5600-rpm engine speeds, the calculated dynamic forces fit perfectly with both the experimental data and the FE results at both the stages of free and forced vibration. It is because that the developed spring model includes the effects of coil clash and variable spring diameter. They are essential for accurately predicting spring forces, especially at the stage of forced vibration, where the compression alters the stiffness of the spring and, thus, the peak spring forces. In addition, it is noted that the developed spring formulas are efficient to couple with the existing modal spring model.

Acknowledgements

This work is funded by Lancaster University through European Regional Development Fund, Centre of Global Eco-Innovation, and industrial partners Force Technology Ltd.

Reference

- [1] J. Guo, W. Zhang, X. Zhang, Y. Cao, Dynamic and exciting analysis with modal characteristics for valve train using a flexible model, *Mechanism and Machine Theory*, 78 (2014) 158-176.
- [2] H. Pawar, D. Desale, Optimization of Three Wheeler Front Suspension Coil Spring, *Procedia Manufacturing*, 20 (2018) 428-433.
- [3] A. Sutrisno, D.J. Braun, How to run 50% faster without external energy, *Science Advances*, 6 (2020) eaay1950.
- [4] S.R. Bullimore, J.F. Burn, Ability of the planar spring–mass model to predict mechanical parameters in running humans, *Journal of Theoretical Biology*, 248 (2007) 686-695.
- [5] S. Patek, M. Rosario, J. Taylor, Comparative spring mechanics in mantis shrimp, *Journal of Experimental Biology*, 216 (2013) 1317-1329.
- [6] A.M. Wahl, *Mechanical springs*, Penton Publishing Company, 1944.
- [7] C. Calder, C. Jenkins, Stress analysis of a helical coil automobile spring using rosettes, *Experimental Techniques*, 12 (1988) 17-20.
- [8] M. Readman, M. Muldoon, L. Reynolds, R. Morris, M. Bayliss, D. Wood, I. Stewart, Control of free length when coiling a helical spring, *IEE Proceedings-Control Theory and Applications*, 148 (2001) 239-244.
- [9] N. Miyamura, T. Kunou, K. Saitoh, Y. Matsumoto, H. Yamamoto, Y. Tsurui, S. Homma, Design and Testing of Ovate Wire Helical Springs, in, *SAE Technical Paper*, 1993.
- [10] F. Ratle, B. Lecarpentier, R. Labib, F. Trochu, Multi-objective optimization of a composite material spring design using an evolutionary algorithm, in: *International Conference on Parallel Problem Solving from Nature*, Springer, 2004, pp. 803-811.
- [11] E. Dragoni, W. Bagaria, Mechanical design of bimaterial helical springs with circular cross-section, *The Journal of Strain Analysis for Engineering Design*, 46 (2011) 304-314.
- [12] S. Seidlitz, Valve train dynamics-a computer study, in, *SAE technical paper*, 1989.
- [13] J. Roß, M. Arnold, Analysis of Dynamic Interactions in Valve Train Systems of IC-Engines by Using a Simulation Model, in, *SAE Technical Paper*, 1993.

- [14] M. Kushwaha, H. Rahnejat, Z. Jin, Valve-train dynamics: a simplified tribo-elasto-multi-body analysis, *Proceedings of the Institution of Mechanical Engineers, Part K: Journal of Multi-body Dynamics*, 214 (2000) 95-110.
- [15] F. Frendo, E. Vitale, L. Carmignani, D. Gagliardi, L. Matteucci, Development of a lumped-parameter model for the dynamic analysis of valve train systems, in, *SAE Technical Paper*, 2004.
- [16] T. Kitada, M. Kuchita, Development of vibration calculation code for engine valve-train, *Mitsubishi Motors Technical Review*, Report, (2008) 74-82.
- [17] J. Guo, W. Zhang, D. Zou, Investigation of dynamic characteristics of a valve train system, *Mechanism and Machine Theory*, 46 (2011) 1950-1969.
- [18] Y. Lin, A.P. Pisano, General dynamic equations of helical springs with static solution and experimental verification, *Journal of applied mechanics*, 54 (1987) 910-917.
- [19] Y. Lin, A.P. Pisano, The differential geometry of the general helix as applied to mechanical springs, *Journal of Applied Mechanics*, 55 (1988) 831-836.
- [20] P. Philips, A. Schamel, J. Meyer, An efficient model for valvetrain and spring dynamics, in, *SAE Technical Paper*, 1989.
- [21] A. Schamel, A frequency domain approach to the analysis and optimization of valve spring dynamics, in, © A. Schamel, 1993.
- [22] A.R. Schamel, J. Hammacher, D. Utsch, Modeling and measurement techniques for valve spring dynamics in high revving internal combustion engines, *SAE Transactions*, (1993) 820-836.
- [23] M. Kumbhalkar, D. Bhoje, A. Vanalkar, P. Chaoji, Failure analysis of primary suspension spring of rail road vehicle, *Journal of failure analysis and prevention*, 18 (2018) 1447-1460.
- [24] N. Lavanya, P.S. Rao, M.P. Reddy, Design and analysis of a suspension coil spring for automotive vehicle, *International Journal of Engineering Research and Applications*, 4 (2014) 151-157.
- [25] H. Liu, D. Kim, Estimation of valve spring surge amplitude using the variable natural frequency and the damping ratio, *International Journal of Automotive Technology*, 12 (2011) 631.

- [26] I. Kacar, V. Yildirim, Free vibration/buckling analyses of noncylindrical initially compressed helical composite springs, *Mechanics Based Design of Structures and Machines*, 44 (2016) 340-353.
- [27] J. Lee, Free vibration analysis of non-cylindrical helical springs by the pseudospectral method, *Journal of Sound and Vibration*, 305 (2007) 543-551.
- [28] F.F. Çalim, Dynamic analysis of composite coil springs of arbitrary shape, *Composites Part B: Engineering*, 40 (2009) 741-757.
- [29] J. Clauberg, R. Huber, Using non-smooth mechanics and parallelization techniques for the efficient simulation of different types of valve springs, in, *SAE Technical Paper*, 2013.
- [30] A.E.H. Love, *A treatise on the mathematical theory of elasticity*, Cambridge university press, 1972.
- [31] A. Yu, Y. Hao, Free vibration analysis of cylindrical helical springs with noncircular cross-sections, *Journal of Sound and Vibration*, 330 (2011) 2628-2639.
- [32] J. Kanimozhi, J. Jothi, T.J. Srinath, M. Jayasimman, D.K. Srinivasan, Design and Analysis of Helical Springs with Non-Circular Cross Section, *International Journal of Latest Technology in Engineering, Management & Applied Science (IJLTEMAS)*, (2018).
- [33] J.M. Renno, B.R. Mace, Vibration modelling of helical springs with non-uniform ends, *Journal of Sound and Vibration*, 331 (2012) 2809-2823.
- [34] H. Liu, D. Kim, Effects of end coils on the natural frequency of automotive engine valve springs, *International Journal of Automotive Technology*, 10 (2009) 413-420.
- [35] G. Chen, J. Zhou, *Vibration and damping in distributed systems*, Crc Press, 1993.
- [36] J. Lee, D. Patterson, Nonlinear valve train dynamics simulation with a distributed parameter model of valve springs, *Journal of engineering for gas turbines and power*, 119 (1997) 692-698.
- [37] Z. Gu, X. Hou, J. Ye, Design and analysis method of nonlinear helical springs using a combining technique: Finite element analysis, constrained Latin hypercube sampling and genetic programming,

Proceedings of the Institution of Mechanical Engineers, Part C: Journal of Mechanical Engineering Science, (2021) 09544062211010210.

[38] Z. Gu, X. Hou, E. Keating, J. Ye, Non-linear finite element model for dynamic analysis of high-speed valve train and coil collisions, International Journal of Mechanical Sciences, (2020) 105476.